NASA Contractor Report

Application of a Two-Layer Near Wall Model to Fully Developed and Rotating Channel Turbulent Flows

C. P. Chen
K. L. Guo

University of Alabama in Huntsville
Huntsville, Alabama 35899.

Final Report

Prepared for
Marshall Space Flight Center
Under Contract NAS8-36955/D.O. 99

November 1991

TABLE OF CONTENTS

LIST OF FIGURES

NOMENCLATURE

C_μ	coefficient for eddy viscosity equation
f_μ	wall damping function
k	turbulence kinetic energy
l_μ	turbulence length scale
l_ϵ	turbulence length scale
Ro	rotation number
Ri	Richardson number
Ri^*	extra term in equation(4)
R_y	turbulent Reynolds number $(k^{1/2}y/\nu)$
R_T	turbulent Reynolds number $(k^2/\nu\epsilon)$
U_j	x_j component of mean velocity
u_j	x_j component of velocity fluctuation
x_j	coordinate direction, 1 - streamwise, 2 - transverse
ϵ	dissipation rate of kinetic energy
ν_t	turbulent viscosity
σ_k	constant in model equation (3)
σ_ϵ	constant in model equation (4)
ω_k	local mean vorticity
Ω	angular velocity

ABSTRACT

The two-layer near wall approach in combination with the $k - \epsilon$ model was applied to rotating flows. Validation studies show that the conventional length scales have to be modified to account for rotating effects. Guided by the Lam and Bremhorst's low Reynolds number model with the rotation-corrected $k - \epsilon$ model, a new set of length scales formulation is proposed. The developments and validations of the current model are reported. A fully elliptic numerical method developed to solve the two-dimensional Reynolds-averaged Navier-Stokes equations is employed for the computational study.

INTRODUCTION

The flow fields in typical liquid rocket engines such as the Space Shuttle Main Engine (SSME) have the common feature that the flow is highly turbulent and the flow paths involve bends through large angles at a small radius of curvature. The flow is normally used to drive turbines during its transit through the system. This implies flows with significant rotation. Experiments concerning the streamwise curvature effects, as well as system rotation effects on turbulence structure have been carried out extensively for the last decade[1,2,3,4]. These effects on shear layers are of considerable interests, both as a basic fluid mechanics problem as well as a design problem for fluid machineries.

For these flow problems involving solid boundaries, the turbulence in the low-Reynolds number near-wall region has been shown to have dominant effects on the overall flow structures. As for the effects of the rotation on the near-wall turbulent structure, Bradshaw[5] in 1969 has pointed out the similarities among rotation, streamline curvature, and thermal stratification on turbulent flows. In all three cases, the extra body force has either a stabilizing or destabilizing effect on the flow depending on its interaction with the driving mechanism. Near the wall regions, these effects are even more profound. Near the concave wall of a curved wall-bounded flow as well as the pressure side wall of a rotating flow, turbulence is significantly enhanced with an increase in the production rate of turbulent kinetic energy. On the other hand, the turbulence is suppressed near the convex wall and even laminarized on the suction side of a rotating flow at high rotational speeds.

There have been a number of computational studies of predicting the rotation as well as streamwise curvature effects on turbulence by using turbulence closure models. While some higher-order models including Reynolds Stress models and Algebraic Stress Models have been used, majority of the models used are eddy viscosity models based on calculations of a characteristic velocity scale and a turbulence characteristics length scale.

For rotating flows and curved flows, the most common form used is the Monin-Obukhov similarity formula (see[5]):

$$\frac{l}{l_0} = \frac{1}{1+\beta Ri} \cong 1 - \beta Ri$$

where β is a constant, which can be determined from experiments, l_0 is the mixing length at zero rotation and in flow with no curvature, and Ri is a Richardson number, defined as

$$Ri = \frac{-2Ro(dU/dy - 2Ro)}{(dU/dy)^2}$$

In which $Ro = \Omega D/U$, Ω is the angular velocity.The Richardson number is a local stability parameter and a negative value of Ri denotes an unstable effect while a positive value denotes a stable effect. For wall-bounded flows, these turbulence models have to be used in conjunction with models dealing with the near-wall low-Reynolds number region.

Several procedures have been developed to provide the near wall treatments which include using wall functions, coupling to some empirical models, and adding low Reynolds correction terms to integrate to the wall. In previous calculations of wall-bounded rotating turbulent flows, wall function approaches [6,7] are most frequently used to model the near-wall region flow structures. These methods are derived from the logarithmic velocity profile based on experimental observations that turbulence at the near-wall region can be described in terms of the wall parameters such as wall shearing stress, normal distances, etc. Therefore, these methods are not valid if the logarithmic velocity profile no longer prevails in the near-wall region. Due to this limited applicability of the wall function methods, low Reynolds number models (see, for example [8]) have been developed to overcome the shortcomings of the wall functions methods. In Ref.[9], we have extended Chien's [10] low Reynolds model for near-wall turbulence structure calculations, to account for rotation/curvature effect. This approach has been shown to be effective in combination with added rotation corrections to the $k-\epsilon$ model. However, a larger number of grid points have to be placed at the near-wall region, and numerical instabilities are frequently

encountered. Another alternative is the two-layer model as described in [11,12]. In this model, the computational domain is divided into two layers near the wall: the outer layer, where the flow is fully turbulent, and the inner layer, where the flow is dominated by viscosity and wall damping effects. The turbulent kinetic energy equations are extended to include the inner layer, whereas the dissipation rate equations are solved only in the outer region. In comparison with the low Reynolds number model, the two-layer model usually requires less grid points in the very near-wall region, and generally is more stable.

The purpose of this study is motivated by the success of the two- layer near wall model for separated flows at low speeds [12], and, for high- speed shock/boundary layer interactions as reported by Horstman [13]. The approach used here is to apply the two-layer near wall treatment to the previously tested rotation-corrected $k-\epsilon$ model of [9]. It was found that the original length scales formulas used in [11,12] based on non-rotating flat plate flow dynamics cannot account for the additional rotation effects in the length scale profiles very close to the wall. New formulations are proposed and tested in this study. The developments and validations are described in the following sections.

GOVERNING EQUATIONS

The Reynolds-averaged momentum equation for incompressible flows on a rotating frame can be written as

$$\frac{\partial U_i}{\partial x_i} = 0 \tag{1}$$

$$\frac{\partial U_i}{\partial t} + \frac{\partial}{\partial x_j}(U_i U_j) = -\frac{1}{\rho}\frac{\partial P}{\partial x_i} + \frac{1}{Re}\frac{\partial}{\partial x_j}(\frac{\partial U_i}{\partial x_j}) - \frac{\partial}{\partial x_j}\overline{u_i' u_j'} - 2\epsilon_{ijk}\Omega_j U_k - (\Omega_j x_j \Omega_i - \Omega_j x_i \Omega_j) \tag{2}$$

The last two terms in equation (2) are the Coriolis and centrifugal forces, respectively, and Ω_i is the angular velocity of the rotating frame. For non-rotating cases, $\Omega_i = 0$.

TURBULENCE MODELING

For turbulent flows the Reynolds equations are closed using an eddy viscosity derived from the $k-\epsilon$ model. The specific turbulence model used here is the one used in our previous study involving a correction term to the ϵ - equation. This two equation model is expressed as:

$$\frac{\partial k}{\partial t}+\frac{\partial}{\partial x_j}(U_j k)=\frac{\partial}{\partial x_j}[(\nu+\frac{\nu_t}{\sigma_k})\frac{\partial k}{\partial x_j}]-\overline{u_i'u_j'}\frac{\partial U_i}{\partial x_j}-\epsilon \tag{3}$$

and

$$\frac{\partial \epsilon}{\partial t}+\frac{\partial}{\partial x_j}(U_j \epsilon)=\frac{\partial}{\partial x_j}[(\nu+\frac{\nu_t}{\sigma_\epsilon})\frac{\partial \epsilon}{\partial x_j}]-C_1\frac{\epsilon}{k}\overline{u_i'u_j'}\frac{\partial U_i}{\partial x_j}$$
$$-C_2(1+Ri^*)\frac{\epsilon^2}{k} \tag{4}$$

$$C_1=1.44$$

$$C_2=1.92$$

The extra term Ri^* that appears in equation (4) is a general Coriolis force modification term which has the form

$$(C_r\omega_k-C_\omega\Omega_k)\Omega_k\frac{k^2}{\epsilon^2}$$

in which $\omega_k=\epsilon_{ijk}(\partial U_i/\partial x_j)$ is the local mean vorticity. The model constants C_r and C_ω were fixed to be 0.406 and 8.802, which gave most satisfactory results for all rotation numbers tested.

The two-layer model concept based on Chen and Patel [9] is used here. The computational domain is divided into two layers near the wall: the outer layer and the inner layer. The turbulent kinetic energy equations are extended to include the inner layer, whereas

the dissipation rate equation is solved only in the outer region. Within the inner layer, ϵ is specified as

$$\epsilon = \frac{k^{3/2}}{l_\epsilon} \tag{5}$$

The eddy-viscosity within this layer is determined as,

$$\nu_t = C_\mu k^{1/2} l_\mu = f_\mu C_\mu \frac{k^2}{\epsilon} \tag{6}$$

where $f_\mu = l_\mu / l_\epsilon$, the length scale l_μ and l_ϵ change exponentially with the turbulence Reynolds number, R_k:

$$l_\mu = C_l n[1.0 - exp(-\frac{R_k}{A_\mu})] \tag{7}$$

$$l_\epsilon = C_l n[1.0 - exp(-\frac{R_k}{A_\epsilon})] \tag{8}$$

$$R_k = \frac{k^{1/2} n}{\nu} \tag{9}$$

where n is the normal distance from the solid wall. To model the effects of wall junctures on the length scale, we follow the procedure commonly used. The resultant length scale l_{eff} is expressed as

$$\frac{1}{l_{eff}} = \sum_{j=1}^{m} \frac{1}{l_j} \tag{10}$$

where m is the number of walls and l_j is the length scale contributed by the j^{th} wall and determined by equation (7) and (8). In the present calculations, the values of constants are determined as follows:

$$C_l = \frac{\kappa}{C_\mu{}^{3/4}} = 2.54 \tag{11}$$

$$A_\epsilon = \frac{2\kappa}{C_\mu{}^{3/4}} = 5.08 \tag{12}$$

Assigning the value of f_μ being 0.95 at the interface of the inner and outer layer, leads to

$$A_\mu = 70 \tag{13}$$

The interface of the inner and outer layer is located along a constant grid line where R_k is greater than 200.

Although the two-layer approach has been shown to be effective for representing pressure gradient effects and provides a more accurate and general description of near-wall flow features than computations using wall functions(see[12]), it has not been applied to a flow where relaminarization occurs near the wall such as the case for suction side of the rotating duct. We first applied the same two-layer model as used for the fully developed channel flow to the rotating duct flow and found that it failed to capture the behavior of outer regions of the inertia sublayer structure due to the rotation effect. The cause is traced back to the formulation of two length scales: i.e. l_μ (which is to be incorporated into ν_t) and l_ϵ (which is to be incorporated into the sink term of the near-wall k-equation). The original formulations of l_μ and l_ϵ were based on flat plate boundary layer formulations without rotation effects. To be consistent with the behavior of Coriolis-modified ϵ-equation near the wall, we have developed an expression to prescribe l_μ and l_ϵ beneath the matched region of the two-layer model. The forms of the l_ϵ and l_μ are given as

$$l_\epsilon = l_{\epsilon 0} \times [1.0 + \gamma(C_r \frac{\partial U}{\partial y} - C_\omega \Omega)\Omega(\frac{k}{\epsilon})^2]^{0.5} \tag{14}$$

$$l_\mu = l_{\mu 0} \times [1.0 + \gamma(C_r \frac{\partial U}{\partial y} - C_\omega \Omega)\Omega(\frac{k}{\epsilon})^2]^{1.5} \tag{15}$$

where $\gamma = 1.30$, These two length scales are then used with Equation (5) and (6) to compute the eddy viscosity within the viscosity-effected region near the wall.

Due to the lack of information about length scales near the rotating surfaces, the guidance of developing the above formulation has been obtained by the asymptotic matching analyses as well as the calculated length scale profiles using the low-Reynolds number

modeling approach. In the study, the rotation-corrected $k-\epsilon$ model (eq.(3) and (4)) are integrated to the wall with the aid of damping functions of Lam and Bremhorst[14]. the advantage of using [14] is that the same model coefficients C_1 and C_2 are used for the two-layer approach. Since the stabilized and destabilized effects are taken care of by the ϵ equations, original functions used by [14] are used here.

RESULTS AND DISCUSSION

The governing differential equations were discretized using finite difference method based on the control-volume formulation on a non-staggered grid arrangement for all dependent variables. The velocity-pressure coupling was resolved by the Operator Splitting method (PISO) in time-marching fashion. The detailed methodology and solution procedure are described in [15]. In principle, this method is capable of computing two-dimensional internal and external flows that are laminar or turbulent, separate or attached, incompressible and compressible, steady or unsteady. The method is stable and requires no smoothing or explicit under-relaxation other than implied by variations in the time step.

The present model was applied to the fully developing channel flow with and without rotations. The computed results will be discussed below.

Fully Developed Channel Flow

The calculations imposed a uniform flow profile at the inlet. Turbulent kinetic energy was set to 0.003 U_{in}^2 and the energy dissipation rate was fixed based on 0.5 channel height or step height. A 86×61 nonuniform grid was used in calculation domain and about 12 grid points were allocated inside the near wall layer. The Reynolds number was 33000 used for the fully developed channel and rotating flows.

The computational results using the standard $k - \epsilon$ model with the two-layer near wall model for the velocity, the turbulent kinetic energy, the dissipation rate, the ratio of production rate and dissipation rate, the ratio of turbulence viscosity and fluid viscosity, the turbulence length scale l_μ and l_ϵ, and the wall damping function f_μ are shown in Figure 1 to Figure 7, respectively. All the profiles plotted in these figures were calculated using three different grids which are 86×47, 86×61 and 86×81. Among these three grid systems, near-wall layer grid points below $y^+ = 100$ is 8, 10 and 12, respectively. It can be found that an 86×61 grid is sufficient to obtain grid independent solutions.

It is noted that the dissipation rate does not vanish in the region very close to the wall. The experimentally observed dissipation rate approaches a constant value in this region. For $y^+ \approx 0$, the dissipation rate takes the limit value $2\nu k/y^2$, which is the analytical solution of the turbulent kinetic energy equation for a limiting case as y approaches zero.

In Figure 4, it is seen that the production rate vanishes at the wall and increase to the peak value at $y^+ \approx 15$. Hence the assumption of equilibrium turbulent flow may not be a good approximation for the region of $y^+ = 0 \sim 30$. Using the vanishing boundary condition for the kinetic energy at the wall yields a growth rate of the turbulent kinetic energy and a production rate that are in good agreement with experimental data as well as theoretical analysis. For the region of $y^+ = 30 \sim 100$, the equilibrium turbulent flow exists since the production rate is approximately equal to the dissipation rate.

From Figure 5, it can be seen that the ratio of turbulent viscosity and fluid viscosity approaches zero at the region $y^+ \approx 10$, which means the flow is laminar. For y^+ greater than 20 the value of the ratio is rapidly increased with linear growth rate. The turbulent viscosity is about 35 times fluid viscosity when y^+ reaches 100.

The wall damping function f_μ shown in Figure 7 is assume to be 0.95 on the interface of the inner and outer layer, where R_k is greater than 200. At the wall, the f_μ takes the limit value of $A_\epsilon/A_\mu \approx 0.073$.

Rotating Channel Flow

For the rotating channel flow, due to different imposed Coriolis accelerations on the pressure and suction sides of rotating boundary layers, rotation exhibits destabilization or stabilization characteristics on the near wall turbulence. At high rotation numbers, the effects on turbulence will lead to eventual laminarization on the suction side and slightly enhancement of turbulence intensities on pressure side in rotating channel flow.

We first present the results using the Lam and Bremhorst low Reynolds near wall damping treatments. At solid walls, no slip conditions and $k = 0$, $d\epsilon/dy = 0$ were imposed. An 81×81 grid was found to be sufficient to obtain grid independent solutions. However, it was noted that sufficient number of grids should be packed within the logarithmic layer near the wall. 20 grid points were required in our calculations with the first grid points away from the wall at about y^+=2.

Figure 8 shows the variation of predicted wall shear velocity with rotation and comparison with the data. The comparison with Johnston's data shows good agreement with the modifying effect on the pressure side of the passage. On the suction side, rotation has significant effect on the near wall turbulence depending on the mean flow Reynolds number.

In Figure 9 and 10, the near wall velocity profiles are plotted in the semi-log form using the wall parameters. Also on the figures is the logarithmic velocity profile. It is seen that fully turbulent flow still exists on the pressure side while laminar flow arises on the suction side due to the stabilizing effect for higher rotation numbers. The drastic effects of rotation on the near wall turbulence and the law-of- the-wall assumption can be further seen from the kinetic energy profiles near both the pressure side wall and suction side wall in Figure 11 and 12. The strong destabilization effects of rotation on the suction side of the rotating wall cause the reduction of turbulent kinetic energy level. For rotation number greater than 0.2, the peaks of turbulent kinetic energy obviously reduce and the turbulent

kinetic energy levels are significantly damped. On the other hand, the destabilizing effects of rotation on the pressure side slightly enhance the turbulent kinetic energy level.

To see the rotation effects on the length scale profiles near walls, l_ϵ and l_μ profiles are plotted vs. y^+ for $Ro = 0.0$ and 0.2 at both suction side and pressure side in Figure 13 to 16. It can be seen that both length scales are drastically effected by rotations. A sequence of runs were performed to derive formulations for length scales as a function of rotation Richardson numbers described in the modeling section. These formulas are then applied for the two-layer approach.

In the low-layer approach, A 86×61 grid was used with 12 grids below the matching regions. From the wall to the matching region, the two length scale formulations were applied to specify eddy viscosities (Eq.(14)) and dissipation rate distributions(Eq.(15)).

In Figure 17 and 18 again, the near wall velocity profiles are plotted in the semi-log form using the wall parameters. Also on the figures is the logarithmic velocity profile. It can been seen that the comparisons are quite good. The effects of rotation on the near wall turbulence can again be seen from the kinetic energy profiles near both the pressure side wall and suction side wall in Figure 19 and 20. In Figure 21 and 22, the turbulence eddy viscosity is plotted for pressure side and suction side, respectively. It shows that the effect of rotating on the turbulence eddy viscosity on the pressure side is small, but on the suction side the effect significantly decreases the value of eddy viscosity. As rotating number approaches 0.2, the eddy viscosity almost becomes zero, which means that only molecular viscosity controls the flow field and no turbulent flow exists on the suction side.

The nondimensional kinetic energy dissipation rate profiles are shown in Figure 23 an 24 for pressure side and suction side. As rotating number increases there is no major change of dissipation rate on the pressure side, but there is a nonmonotonous change existed on the suction side. It has been shown that the dissipation rates decrease for small rotating number(< 0.1), and increase for large rotating number. According to our experince of

using low-Reynolds number treatment, such increasing seems to be very sharply and reach the much larger when rotating number greater than 0.1.

The length scale l_ϵ and l_μ profiles are plotted in Figure 25 to Figure 28. As rotating number increases, the length scales do not change much on the pressure side wall. However, on the suction side, the length scale l_μ becomes smaller and l_ϵ does not change too much as rotation number increases.

CONCLUDING REMARKS

Validation studies of the rotation-corrected $k - \epsilon$ turbulence model in combinations with a near-wall two-layer model are carried out. A fully developed channel flow was first calculated to establish the issues of matching points, matching criteria based on local turbulence Reynolds numbers, eddy viscosity ratios and grid point resolutions beneath the matching point. Then, the two-layer approach was applied to the rotating channel flow case. It was found that the original formula for length scales at the matching point of the outer layer and inner layer cannot be applied to the complex near wall turbulence structures due to flow system rotation. A new formula for both length scales, guided by the Lam and Bremhorst damping function model, was proposed and validated in this study. It is shown that with proper corrections in length scale formulations, good predictions of near wall turbulence can be obtained. It is recommended that current formula should be further generalized for highly curved and separated flows.

ACKNOWLEDGEMENTS

The authors wish to acknowledge the computer time supplied by the Alabama Surper-computer Network through UAH Computer Services.

REFERENCES

1. Bardina, J., Ferziger, J.H. and Rogallo, R.S., "Effect of Rotation on Isotropic Turbulence: Computation and Modeling," J. Fluid Mech. , **154**, 321-336, 1985.
2. Johnston, J.P. et al., "Effects of Spanwise Rotation on Structure of 2-D fully Developed Turbulent Channel Flow," J. Fluid Mech. , **56**, 533, 1972.
3. Muck, K.C., Hoffman, P. H. and Bradshaw, P., "The Effect of Convex Surface Curvature on Turbulent Boundary Layer," J. Fluid Mech. , **161**, 347-369, 1985.
4. Hoffman, P., H. Muck, K.C. and Bradshaw, P., "The Effect of Concave Surface Curvature on Turbulent Boundary Layer," J. Fluid Mech. , **161**, 371-403, 1985.
5. Bradshaw, P., "The analogy Between Streamline Curvature and Buoyancy in Turbulent Shear Flow," J. Fluid Mech., **36**, part 1, 177-191, 1969.
6. Howard, J.H., Patankar, S.V. and Bordynuik, R.M., "Flow Prediction in Rotating Ducts Using Coriolis-Modified Turbulence Models,"ASME J. Fluid Eng. , **102**, 456, 1980.
7. Lakshminarayana, B., "Turbulence Modeling for Complex Shear Flows," AIAA J. , **24**, 1990, 1986.
8. Patel, V. C., Rodi, W. and Scheuerer, G., "Turbulence Model for Near-Wall and Low Reynolds Number Flows: A Review ", AIAA J. , **89** 1308-1319, 1985.
9. Chen, C. P. and Guo, K. L., " Low Reynolds Number Turbulence Modeling of Rotating Flows ", Forum on Turbulent Flows-1990, FED-**94**, 29-33, 1990.
10. Chien, K. Y., " Predictions of Channel and Boundary Layer Flows with a Low Reynolds Number Turbulence Model ", AIAA J. ,**20**, 33-38, 1982.
11. Chen, H. C. and Patel, V. C., " Near-Wall Turbulence Models for Complex Flows Including Separation ", AIAA J. ,**26**, 641-648, 1988.
12. Rodi, W., "Experience with Two-Layer Models Combining the $k-\epsilon$ Model with a One-Equation Model Near the Wall ", AIAA paper 91-0216, 1991.
13. Horstman, C. C., "Hypersonic Shock-wave Turbulent-Boundary- Layer Interaction Flow - Experiment and Computation," AIAA paper 91-1760, 1991.
14. Lam, C.K.G. and Bremhorst, K., "A Modified Form of the k-ϵ Model for Predicting Wall Turbulence," ASME J. Fluid Eng. , **103**, 456-460, 1981.
15. Jiang, Y., Chen, C.P. and Chyu M.K., "A Numerical Computation of Convective Heat Transfer in Two-Pass Rectangular Channel With a 180-Degree Sharp Turn," AIAA paper 90-0355, 1990.

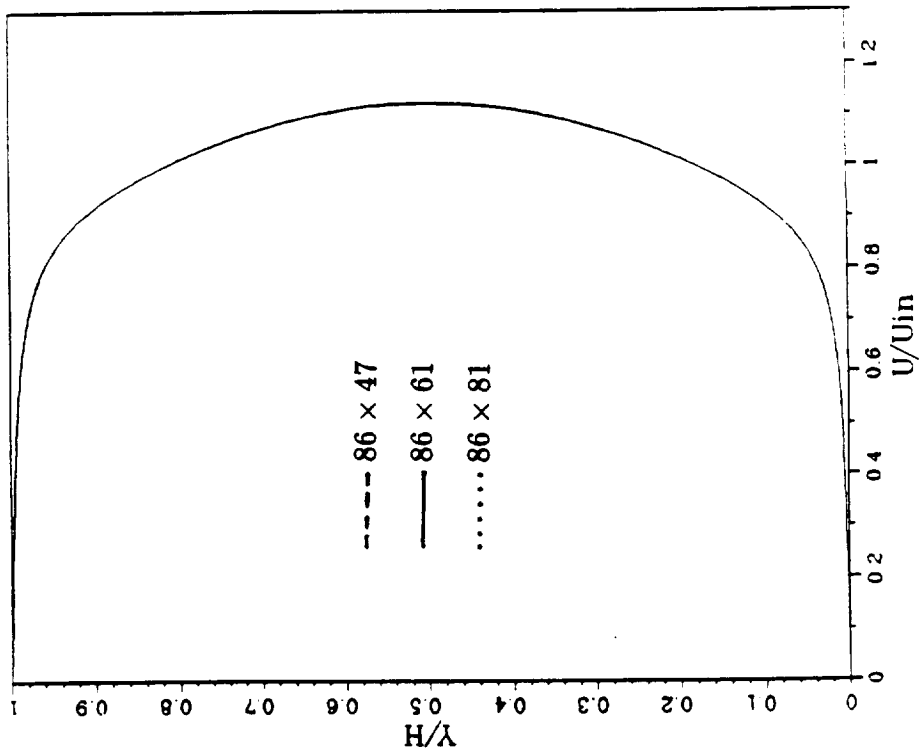

Figure 1

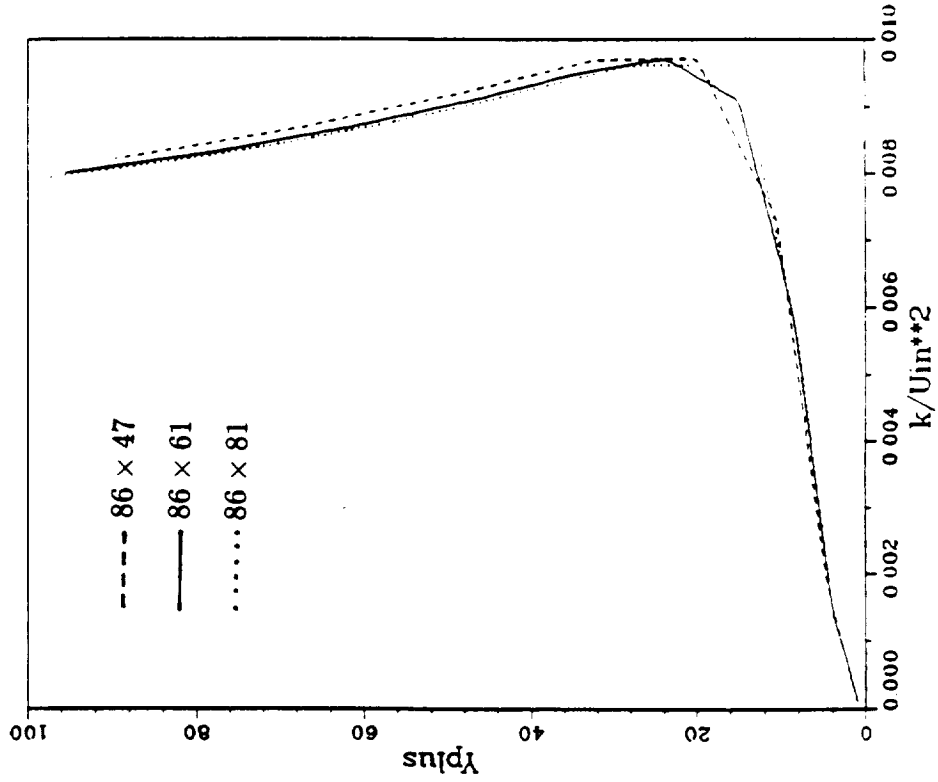
86 × 47
86 × 61
86 × 81
Yplus
k/Uin**2
0
20
40
60
80
100
0.000
0.002
0.004
0.006
0.008
0.010

Figure 2

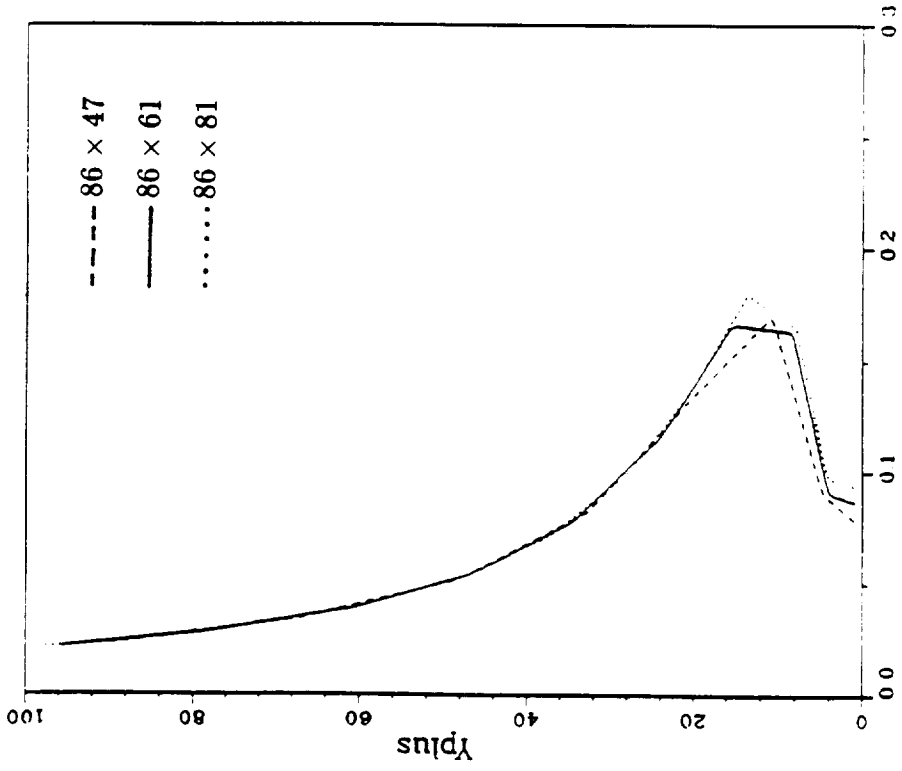

Figure 3

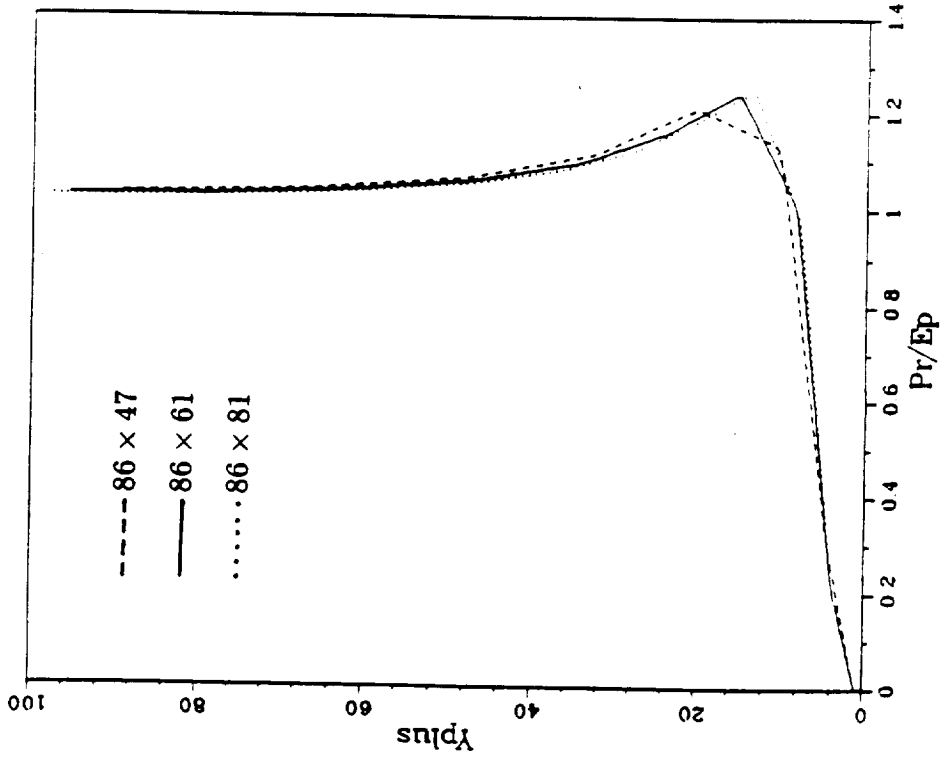

Figure 4

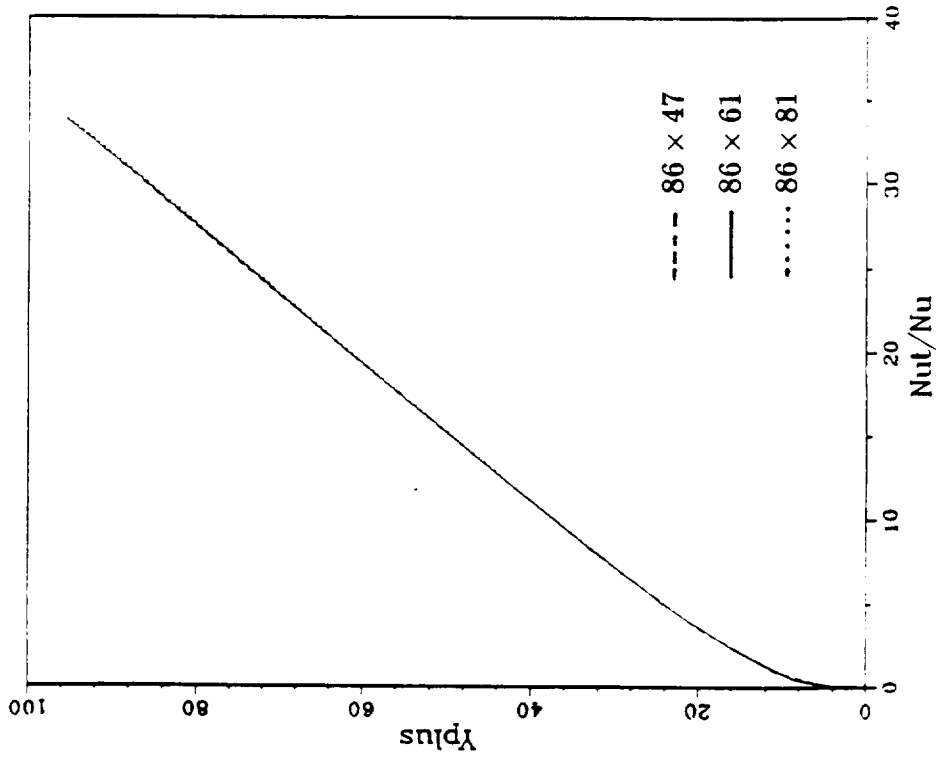

Figure 5

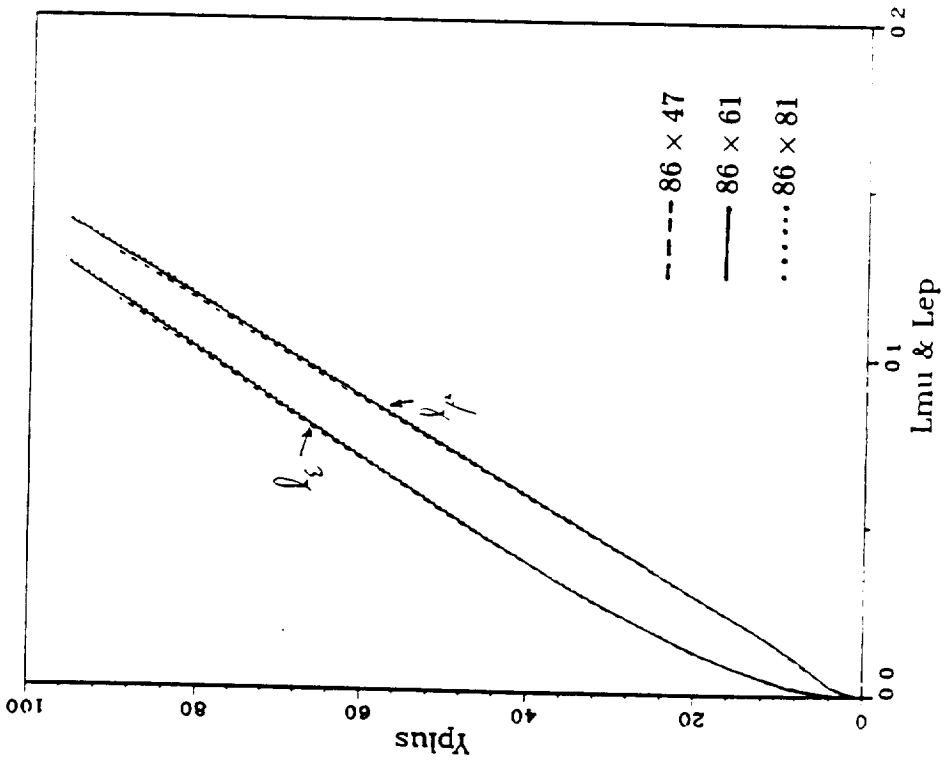

Figure 6

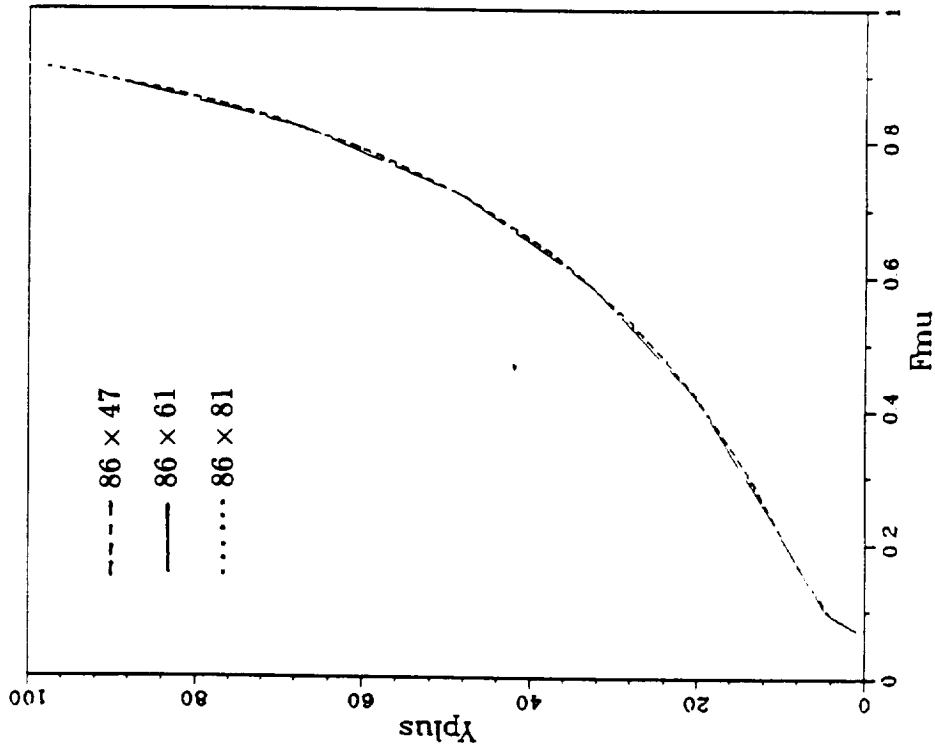

Figure 7

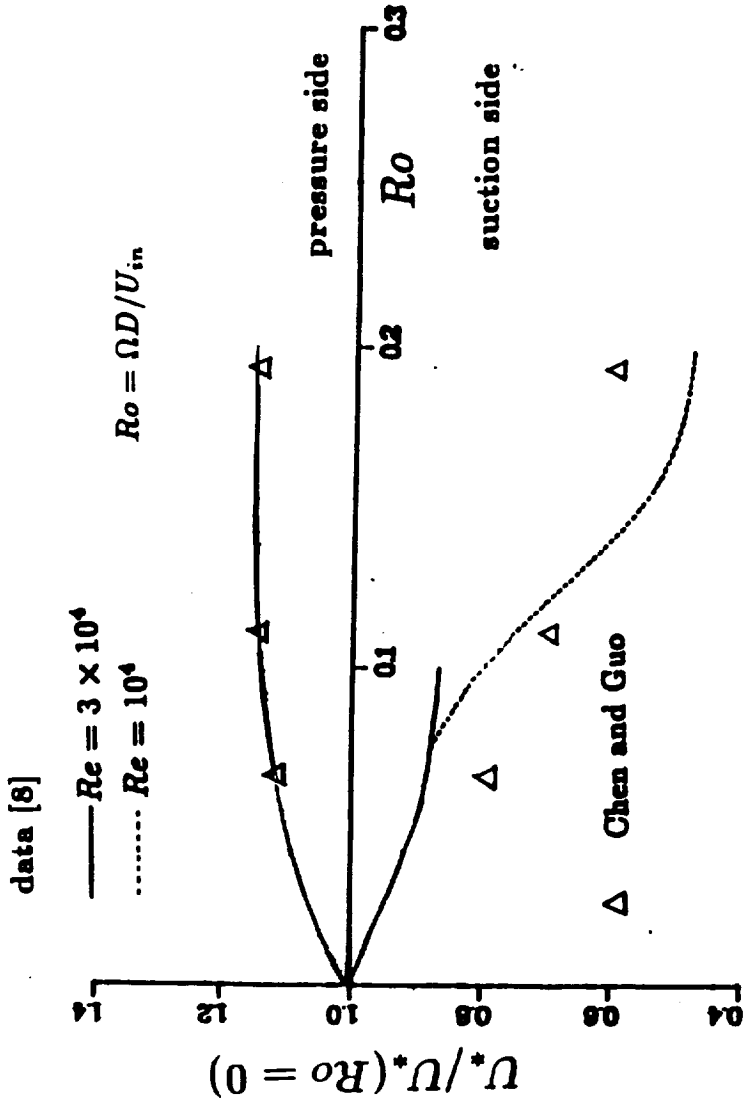
data [8]
$Re = 3 \times 10^4$
$Re = 10^4$
$Ro = \Omega D/U_{in}$
pressure side
suction side
Ro
Chen and Guo
$U_*/U_*(Ro = 0)$
1.4
1.2
1.0
0.8
0.6
0.4
0.3
0.2
0.1

Figure 8

THE NEAR WALL VELOCITY PROFILE IN ROTATING DUCT

pressure side

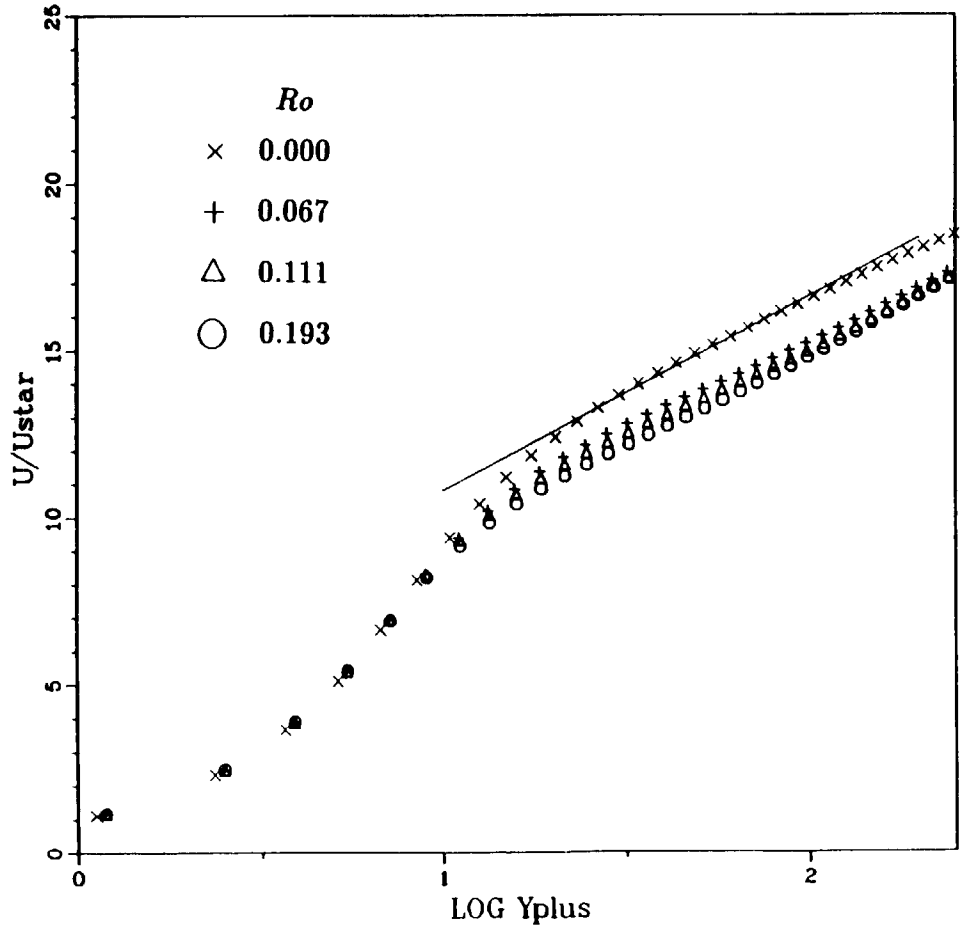

Figure 9

THE NEAR WALL VELOCITY PROFILE IN ROTATING DUCT

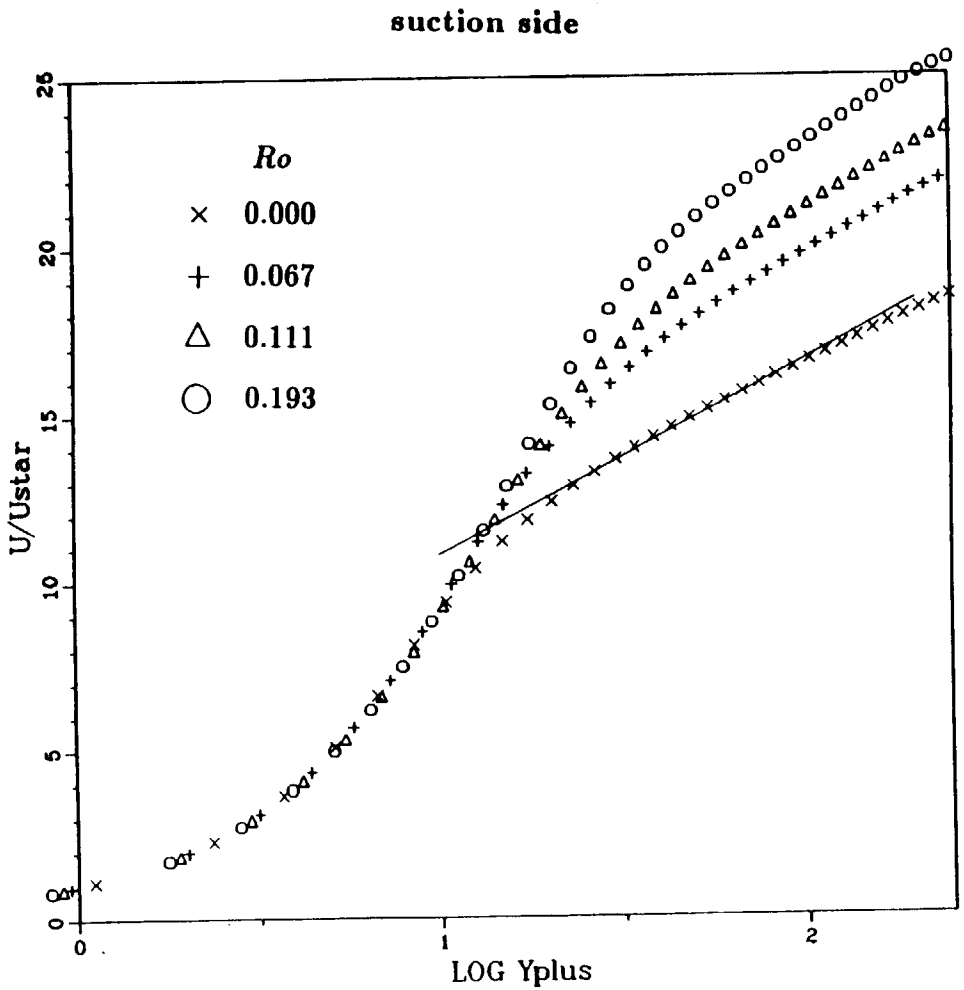

Figure 10

THE KINETIC ENERGY PROFILE IN ROTATING DUCT

pressure side

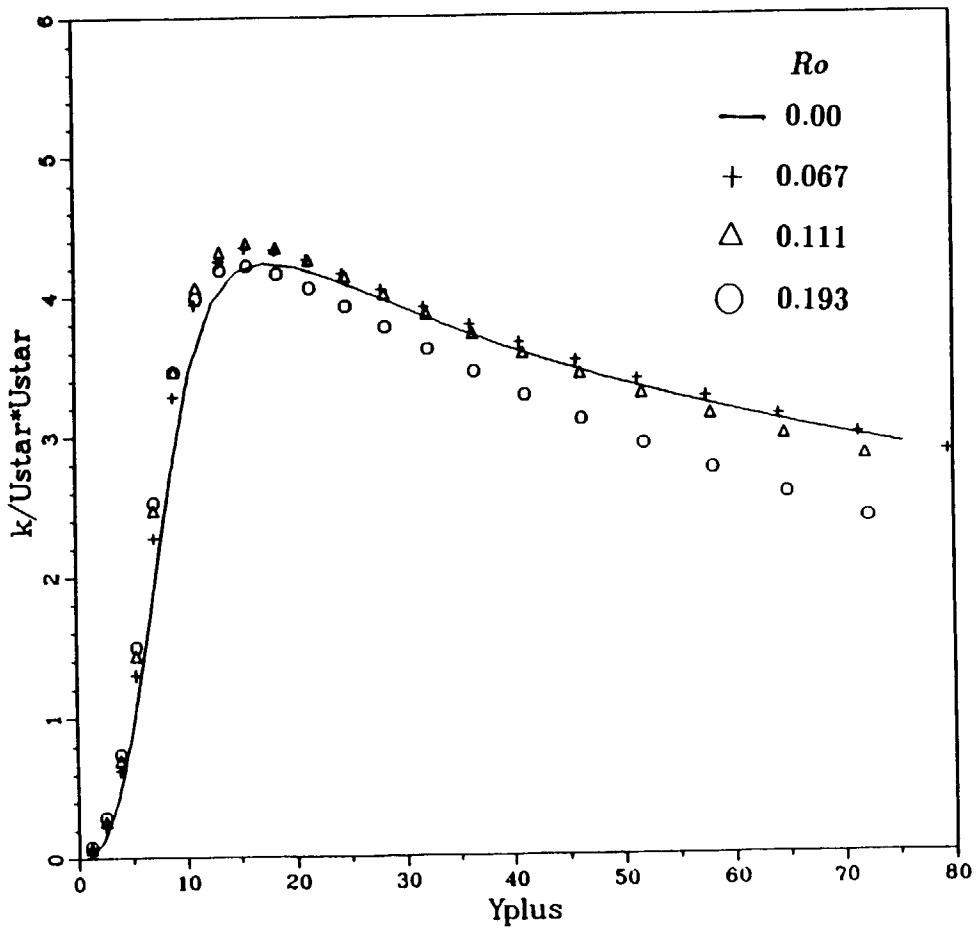

Figure 11

THE KINETIC ENERGY PROFILE IN ROTATING DUCT

suction side

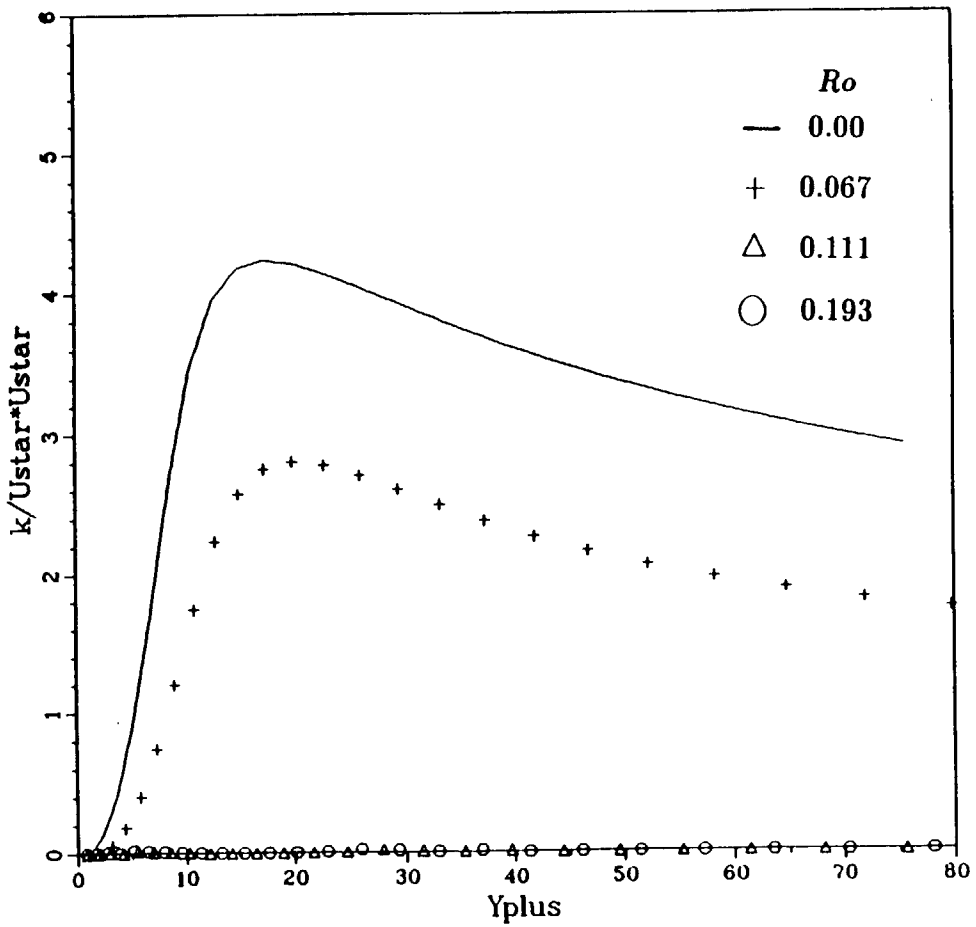

Figure 12

LENGTH SCALE PROFILE IN ROTATING DUCT

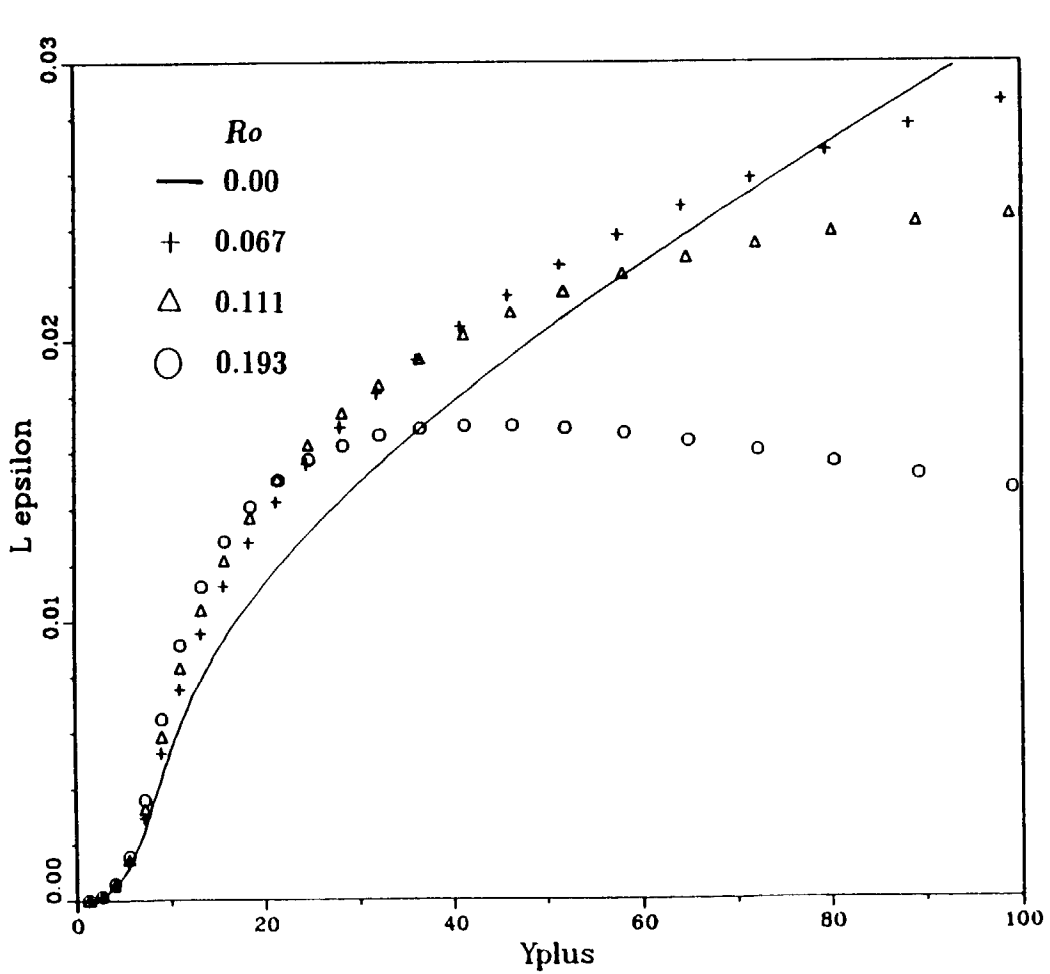

Figure 13

LENGTH SCALE PROFILE IN ROTATING DUCT

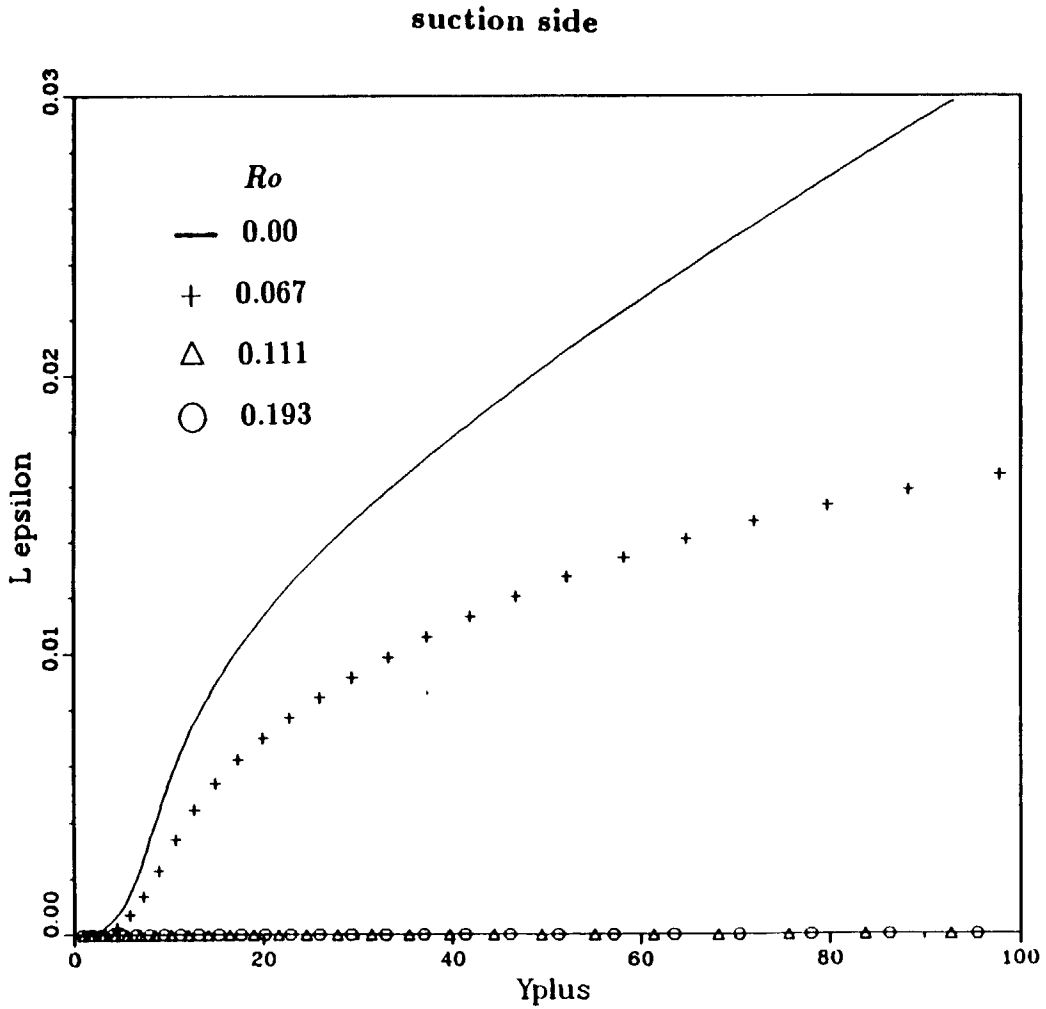

Figure 14

LENGTH SCALE PROFILE IN ROTATING DUCT

pressure side

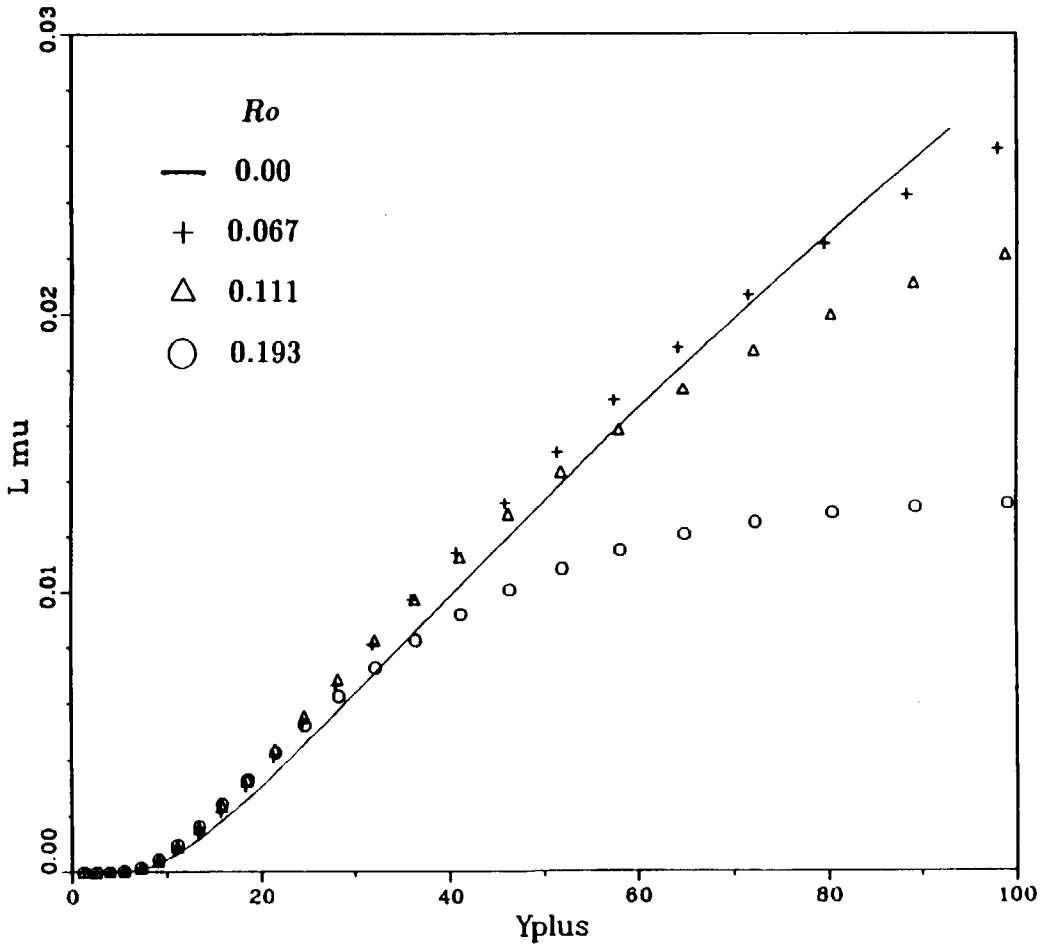

Figure 15

LENGTH SCALE PROFILE IN ROTATING DUCT

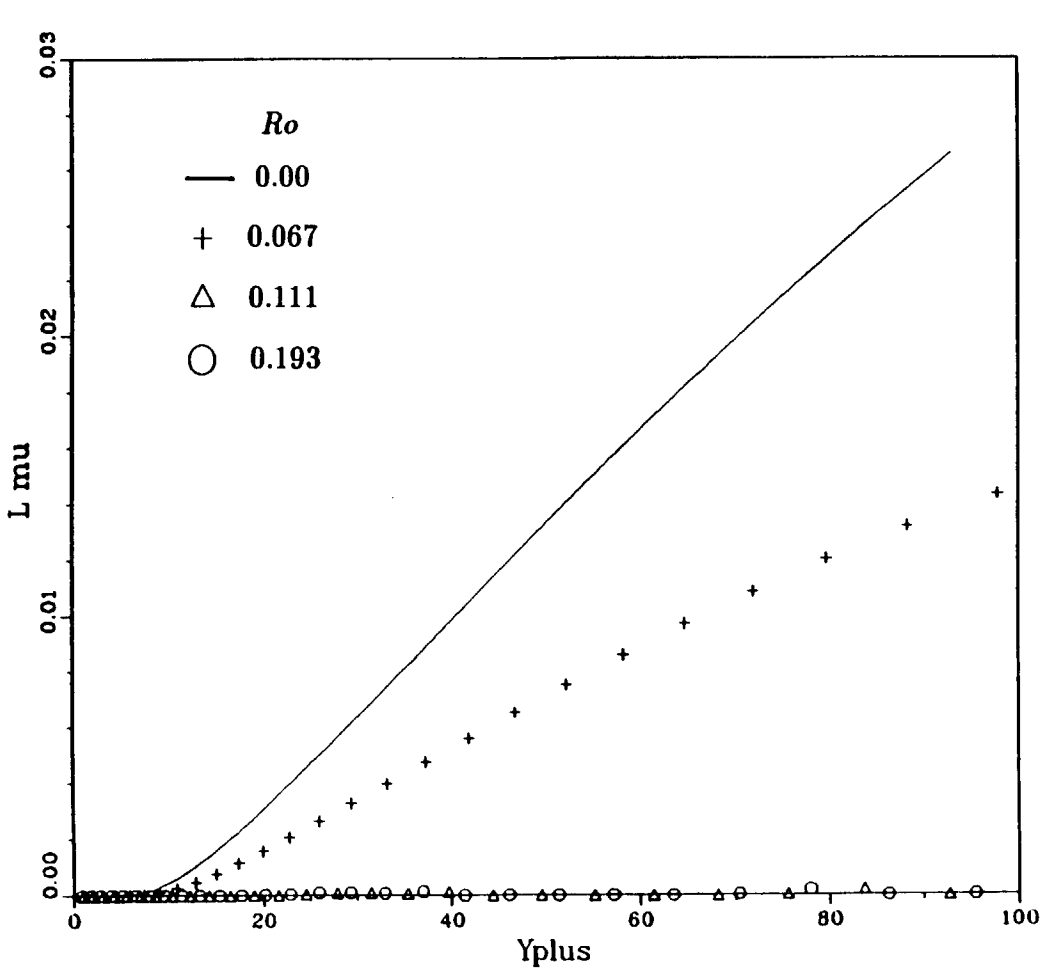

Figure 16

THE NEAR WALL VELOCITY PROFILE IN ROTATING DUCT

pressure side

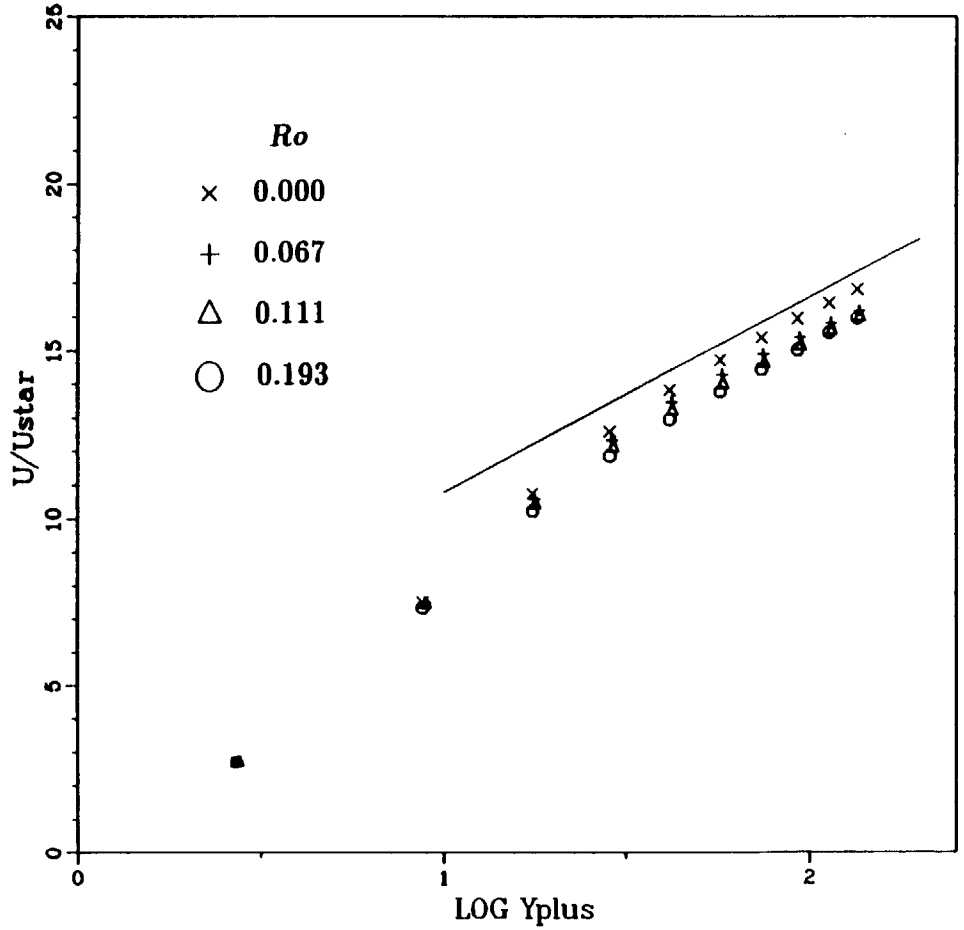

Figure

THE NEAR WALL VELOCITY PROFILE IN ROTATING DUCT

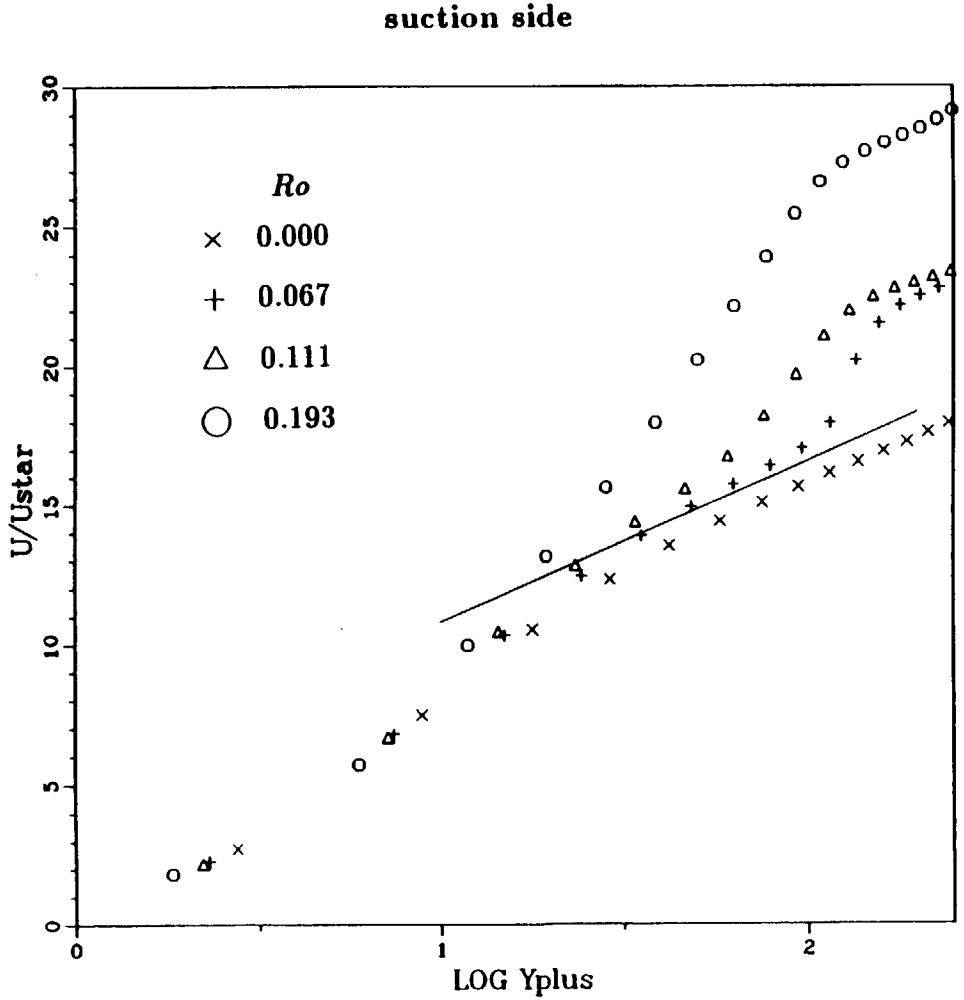

Figure

KINETIC ENERGY PROFILE IN ROTATING DUCT

pressure side

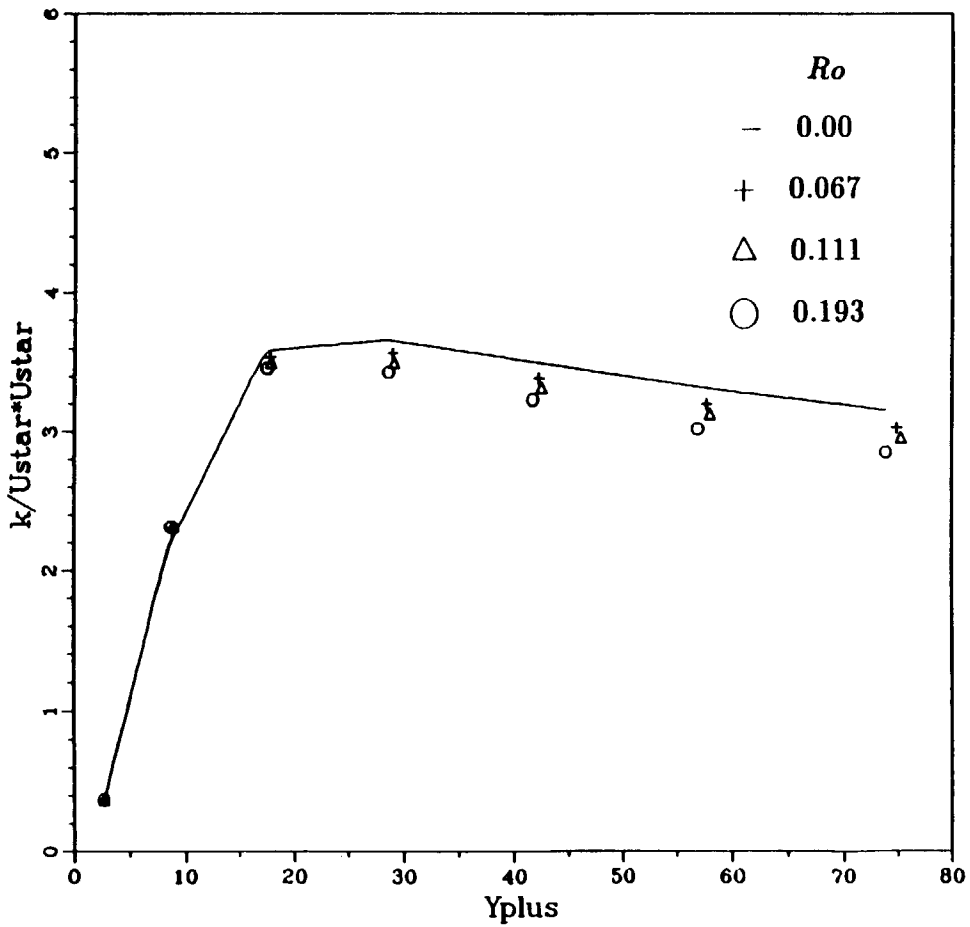

Figure 3

KINETIC ENERGY PROFILE IN ROTATING DUCT

suction side

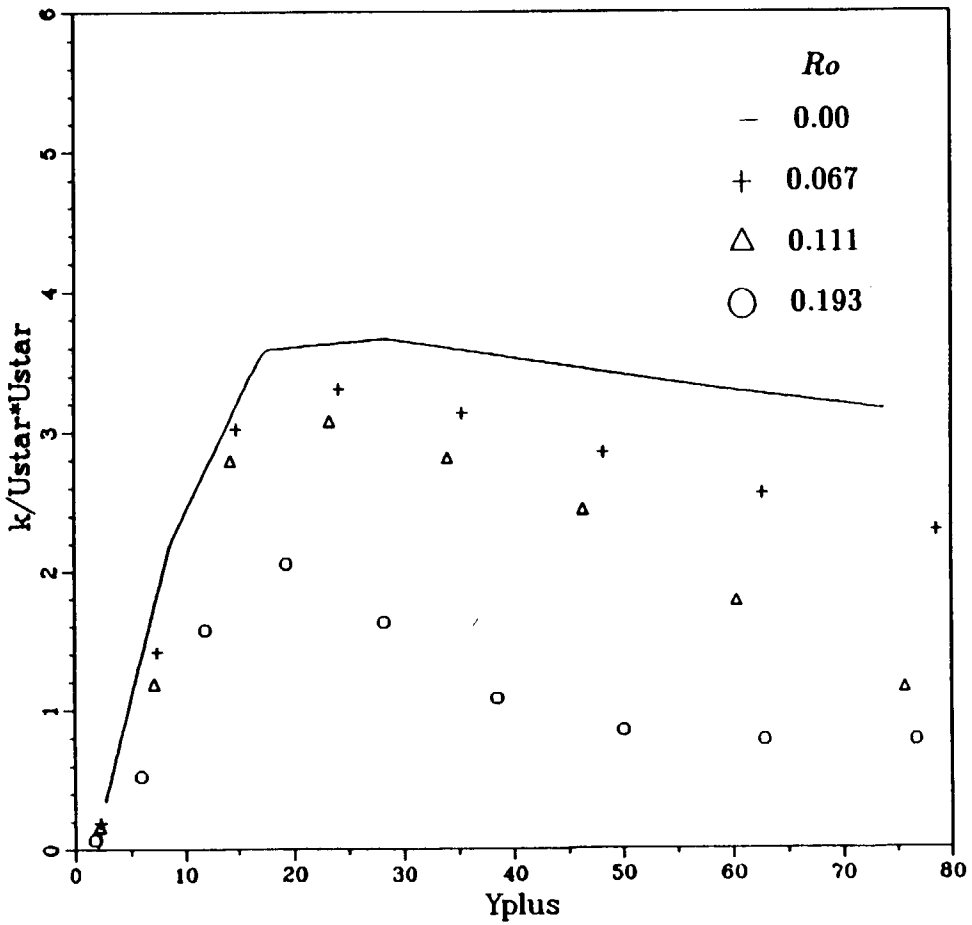

Figure

EDDY VISCOSITY PROFILE IN ROTATING DUCT

pressure side

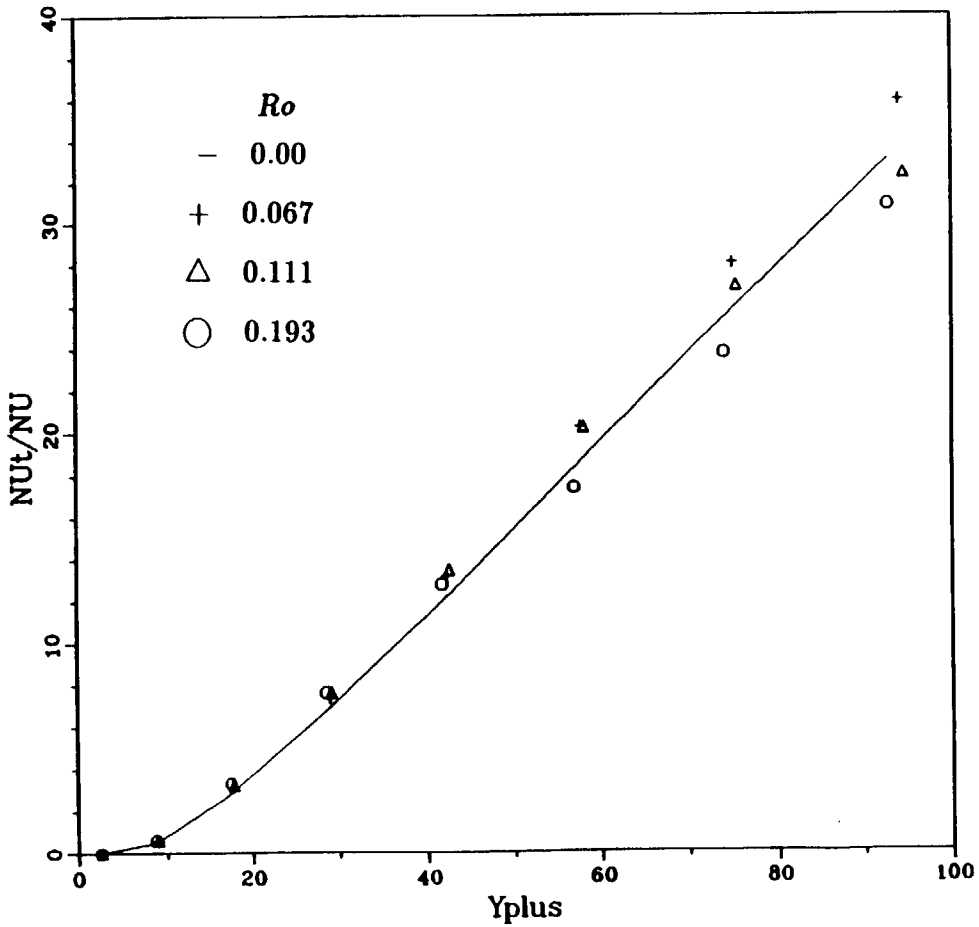

Figure 21

EDDY VISCOSITY PROFILE IN ROTATING DUCT

suction side

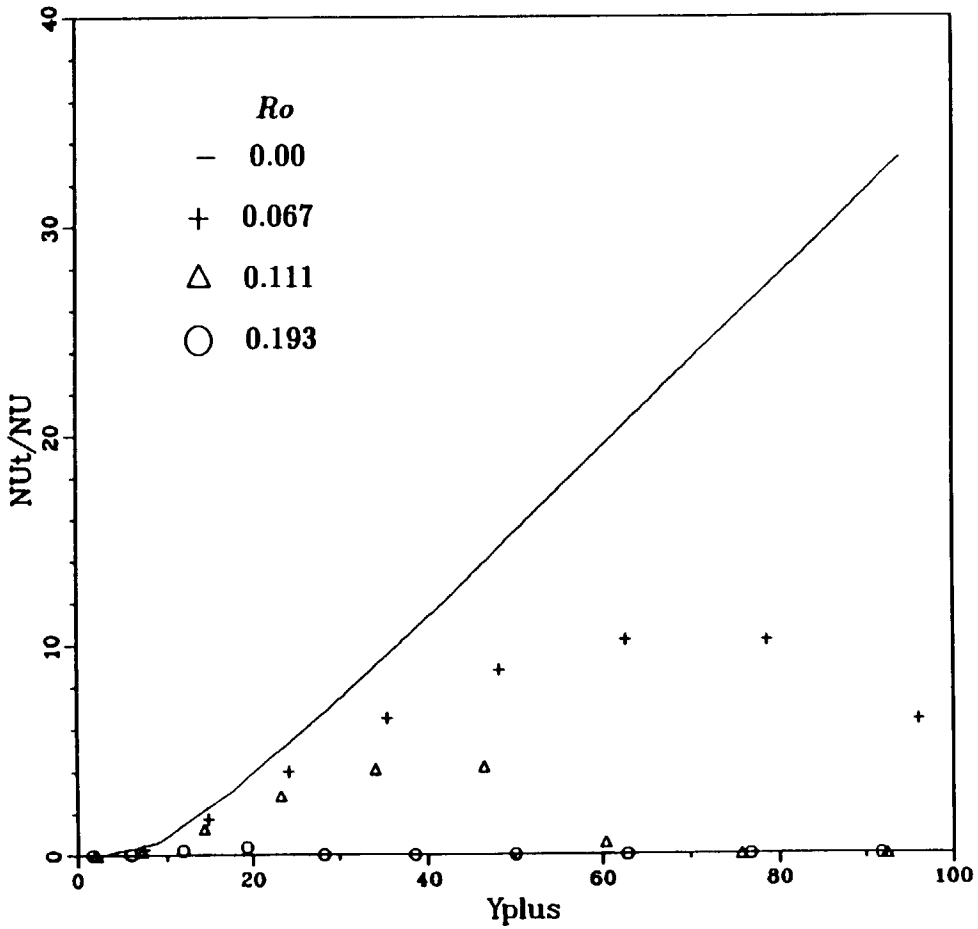

Figure 22

DISSIPATION RATE PROFILE IN ROTATING DUCT

pressure side

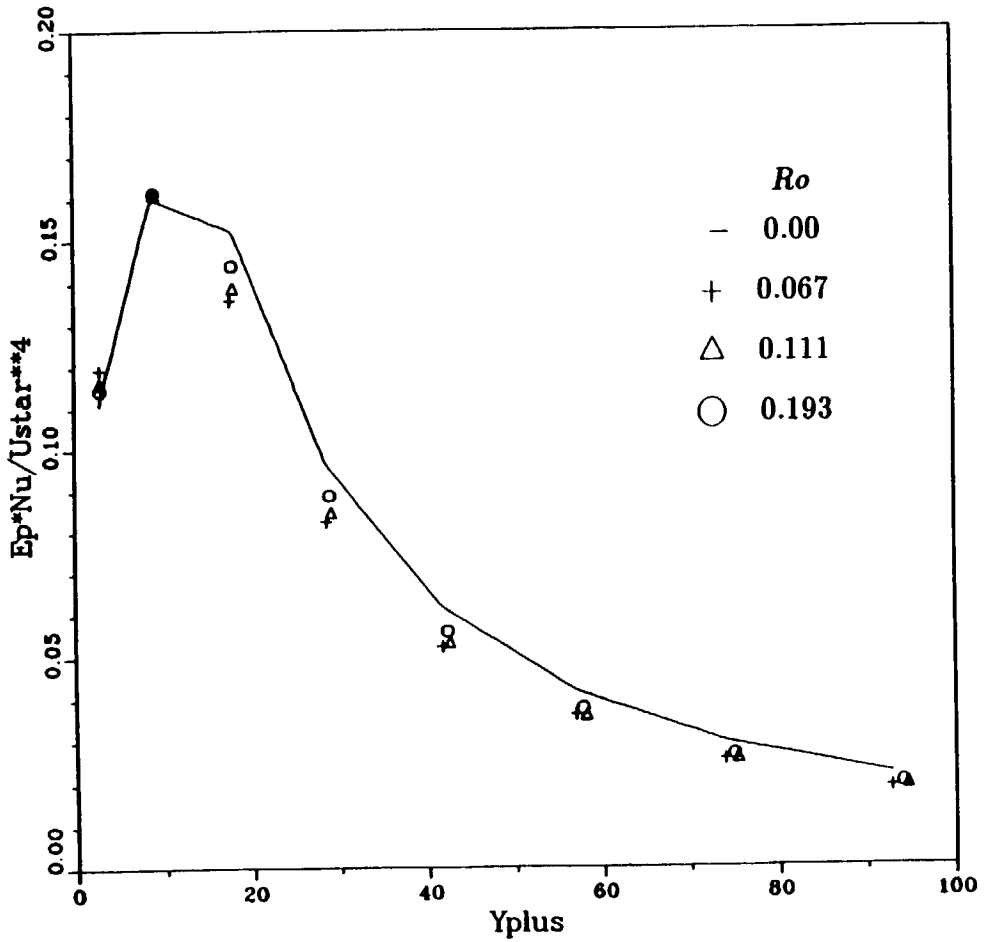

Figure 23

DISSIPATION RATE PROFILE IN ROTATING DUCT

suction side

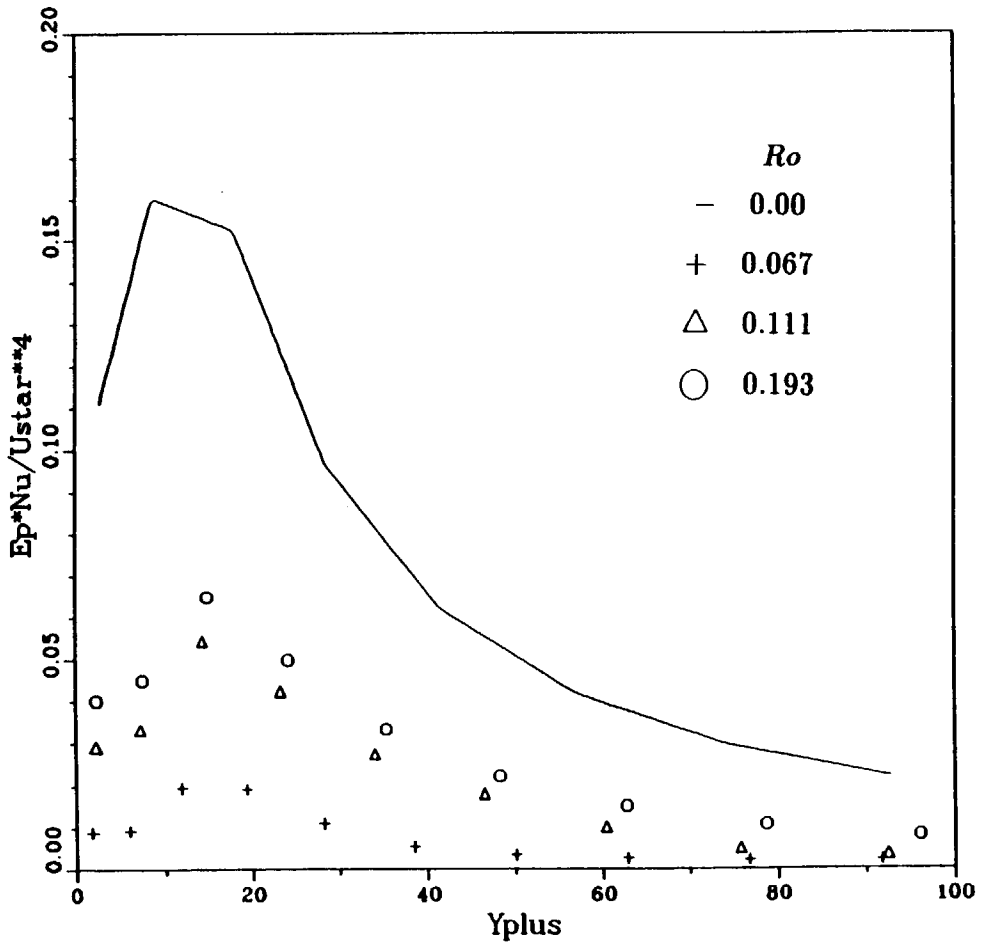

Figure 24

LENGTH SCALE PROFILE IN ROTATING DUCT

pressure side

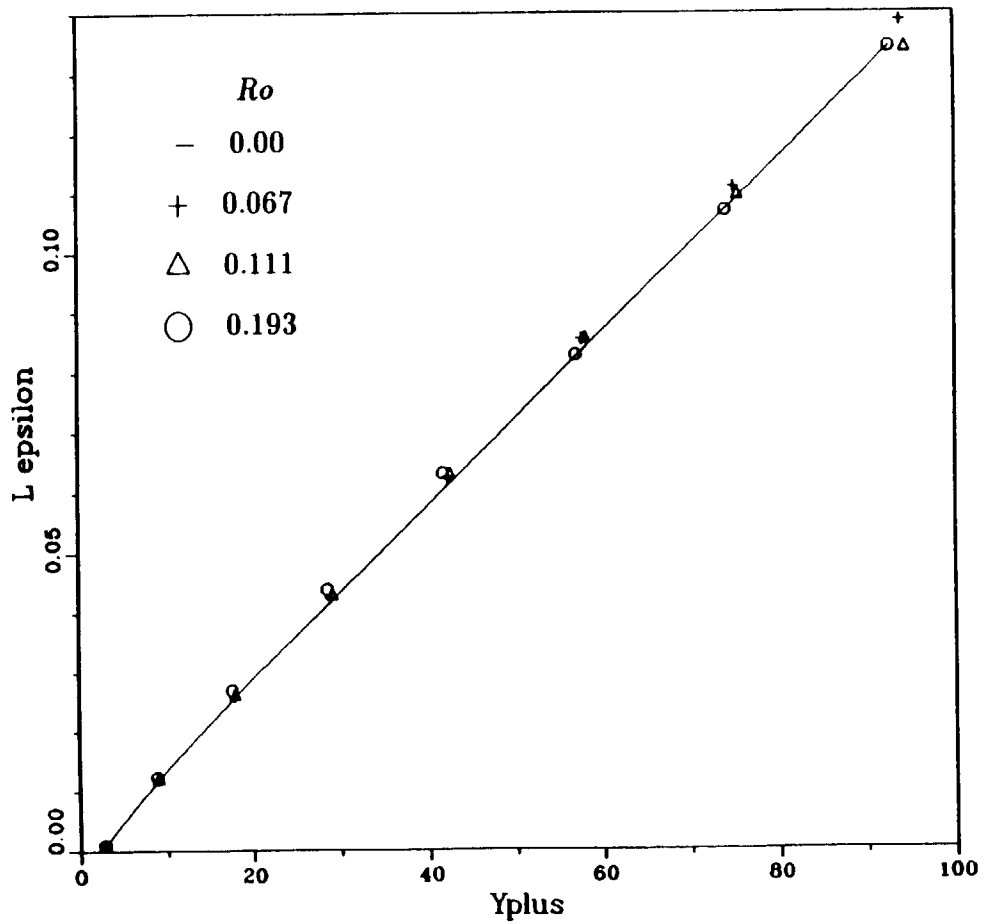

Figure 25

LENGTH SCALE PROFILE IN ROTATING DUCT

suction side

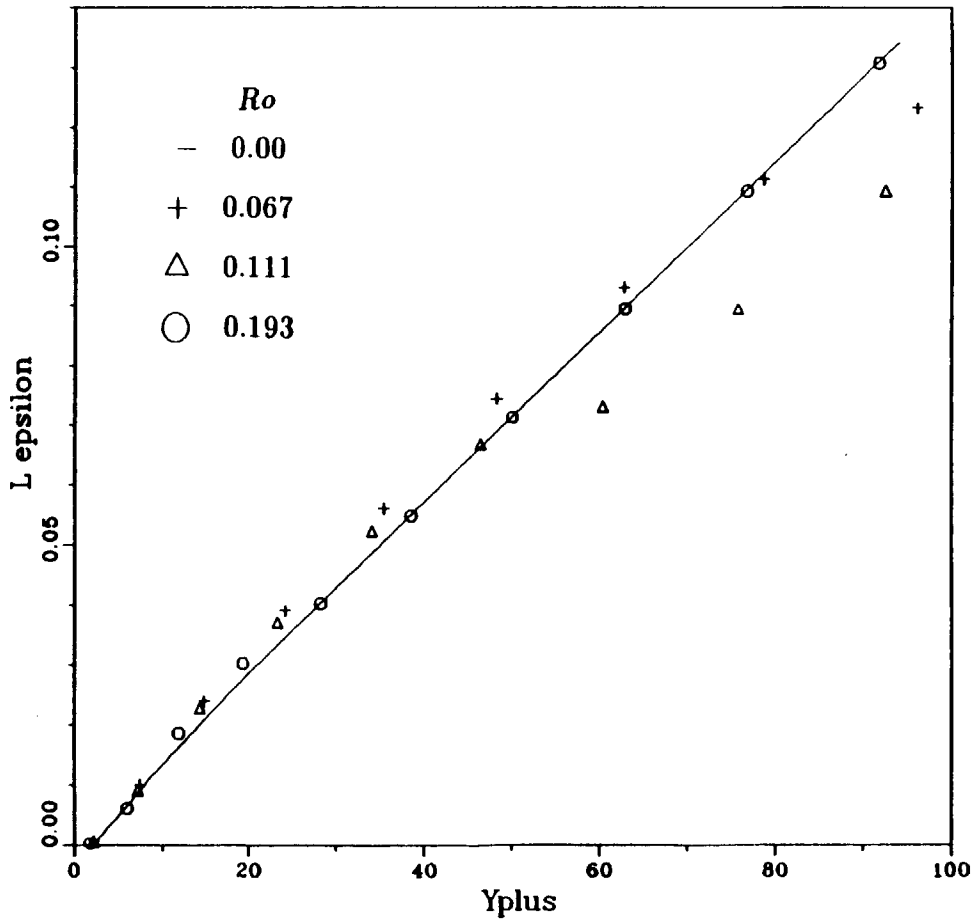

Figure 26

LENGTH SCALE PROFILE IN ROTATING DUCT

pressure side

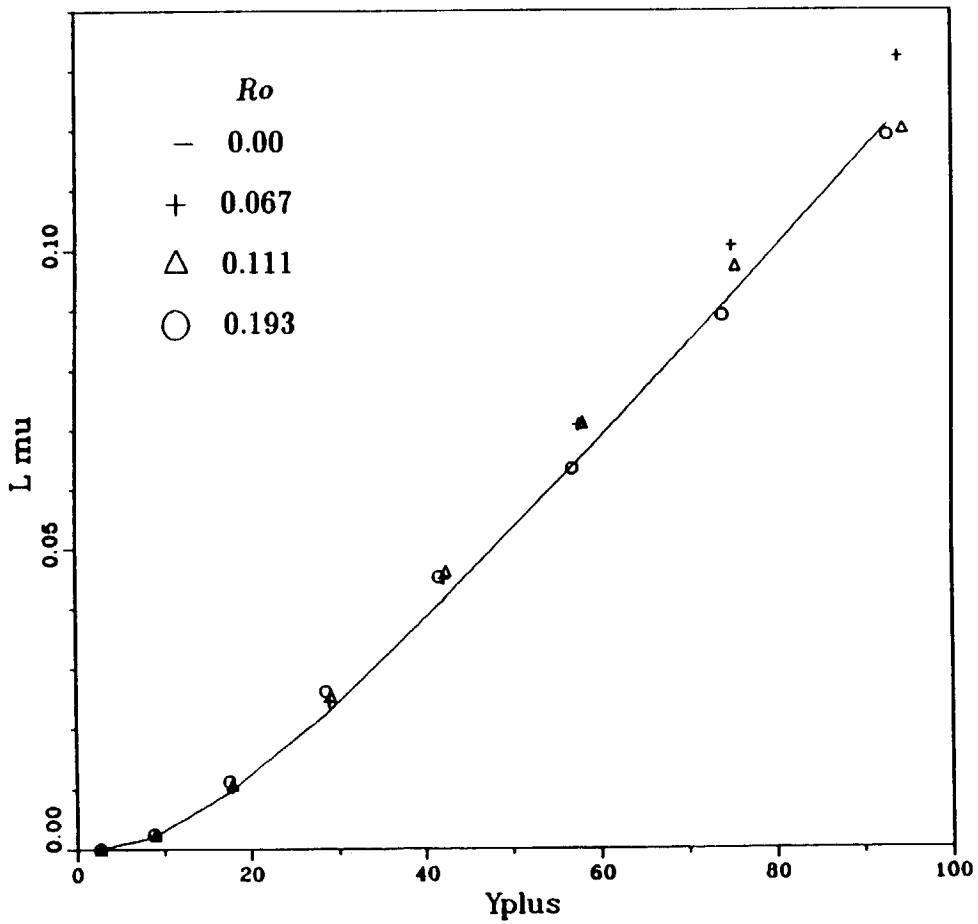

Figure 27

LENGTH SCALE PROFILE IN ROTATING DUCT

suction side

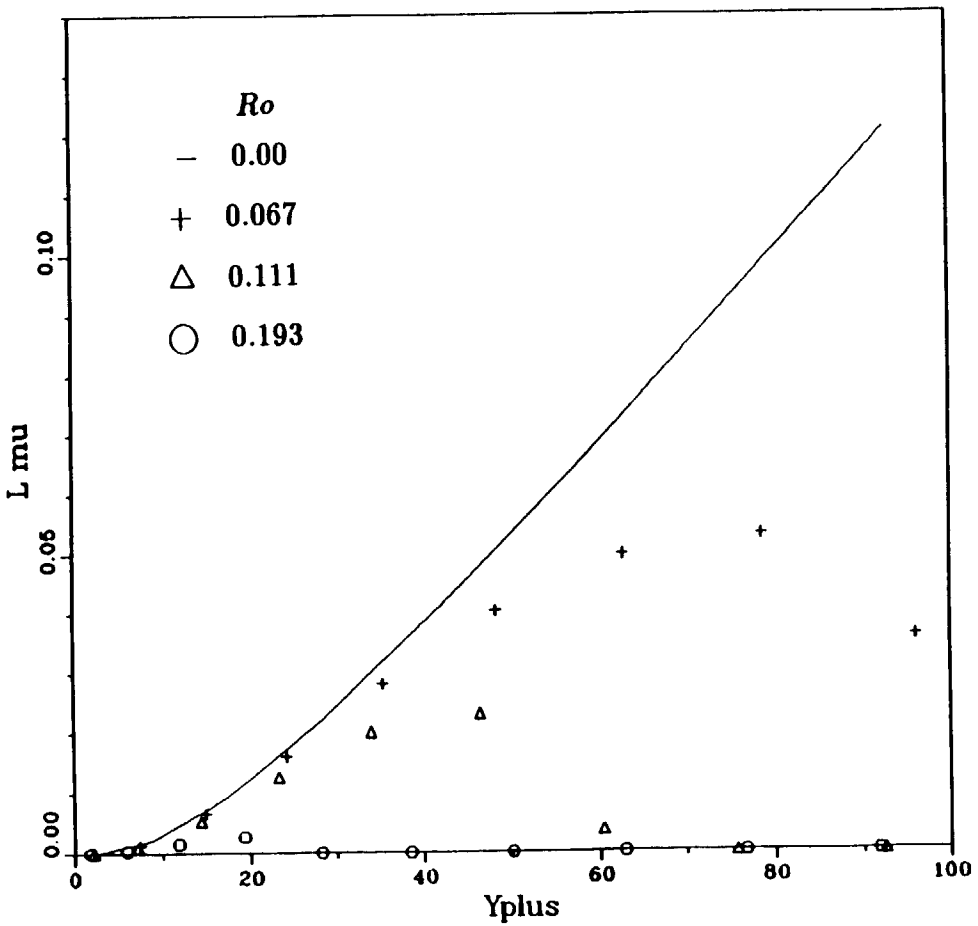

Figure 28